A MULTIPLE FLARE SCENARIO WHERE THE CLASSIC LONG DURATION FLARE WAS NOT THE SOURCE OF A CME

C.P. GOFF[1], L. van DRIEL-GESZTELYI[1,2,3], P. DÉMOULIN[2], J.L. CULHANE[1], S.A. MATTHEWS[1], L.K. HARRA[1], C.H. MANDRINI[4], K.L. KLEIN[2], H. KUROKAWA[5]

[1] *Mullard Space Science Laboratory, University College London, Holmbury St. Mary, Dorking, Surrey, RH5 6NT, U.K.*
*(*chris@chrisgoff.co.uk, lvdg@mssl.ucl.ac.uk*)*

[2] *Observatoire de Paris, LESIA, UMR 8109 (CNRS), F-92195 Meudon Principal Cedex, France*

[3] *Konkoly Observatory of the Hungarian Academy of Sciences, Budapest, Hungary*

[4] *Instituto de Astronomía y Física del Espacio, CONICET-UBA, CC. 67, Suc. 28, 1428 Buenos Aires, Argentina*

[5] *Hida and Kwasan Observatories, Kyoto University, Yamashina, Kyoto 607, Japan*

Received ; accepted

Abstract. A series of flares (GOES class M, M and C) and a CME were observed in close succession on 20th January 2004 in NOAA 10540. Radio observations, which took the form of types II, III and N bursts, were associated with these events. We use the combined observations from TRACE, EIT, Hα images from Kwasan, MDI magnetograms, and GOES to understand the complex development of this event.
Contrary to a standard interpretation, we conclude that the first two impulsive flares are part of the CME launch process while the following LDE flare represents simply the recovery phase. Observations show that the flare ribbons not only separate but also shift along the magnetic inversion line so that magnetic reconnection progresses stepwise to neighbouring flux tubes. We conclude that "tether cutting" reconnection in the sheared arcade progressively transforms it to a twisted flux tube which becomes unstable, leading to a CME. We interpret the third flare, a long-duration event, as a combination of the classical two-ribbon flare with the relaxation process following forced reconnection between the expanding CME structure and neighbouring magnetic fields.

1. Introduction

Long duration events (LDE) are strongly linked to classical two ribbon flares, which develop after filament eruptions. The two flare ribbons are connected by flare loops, which represent field lines reconnected in the current sheet formed in the wake of the erupting filament. LDEs therefore are considered eruptive flares and have a strong link to CMEs (Sheeley *et al.*, 1983). Early studies using Skylab and SMM data revealed a high percentage (> 80 %) of associations between CMEs, filament eruptions and LDEs (Webb and Hundhausen, 1987). Impulsive flares can also be eruptive (see e.g. Nitta and

Hudson, 2001), though they are traditionally linked to quadrupolar confined flares. Some flares can be hybrids, having both confined and eruptive characteristics (Švestka, 1989).

Quadrupolar flares appear as four individual ribbons that are located at the footpoints of field lines having four independent connectivities. Topological analyses and models of quadrupolar confined (non-eruptive) flares have been developed by, e.g., Mandrini *et al.* (1991), Démoulin *et al.* (1993), and Melrose (1997). The latter paper was based on the reconnection of two current carrying magnetic loops. 3D reconnection of the two interacting loops does not involve any opening of field lines; thus no CME is involved in these cases.

A different quadrupolar flare/CME model was developed by Antiochos, DeVore, and Klimchuk (1999). Here a central arcade is increasingly sheared, and therefore rises against the overlying field. At some time during the evolution, magnetic reconnection is triggered, resulting in a weakening of the overlying field-line tension. Thus, the sheared core field can burst through creating a CME. This process is called "magnetic breakout".

Several flare/CME models were also developed for bipolar configurations. One basic physical idea is that reconnection can occur when a magnetic arcade is sufficiently sheared. This reconnection transforms the sheared arcade progressively into a twisted flux tube and a small scale arcade under the twisted flux tube. Reconnection continues to cut the stabilizing anchorage of the arcade field lines in the photosphere, removing the tethers (e.g. van Ballegooijen and Martens, 1989; Inhester, Birn, and Hesse, 1992; Moore, Larosa, and Orwig, 1995; Moore *et al.*, 2001; Amari *et al.*, 2003; Shiota *et al.*, 2005). Such models, where reconnection occurs below the forming twisted flux tube, are broadly referred to as tether cutting models. At some point in the evolution the strength of the remaining anchored field becomes sufficiently weakened to allow the configuration to reach an unstable point, leading to an eruption (e.g. Martens and Kuin, 1989; Lin *et al.*, 1998). Another class of models involves photospheric twisting motions. In these models a kink instability is triggered when the twist exceeds a critical threshold (e.g. Török and Kliem, 2003).

Depending on the event studied, observations may not fall neatly into one of the above categories. The localization of the flare ribbons in confined events is well understood from the computed magnetic topology of the configuration (see Démoulin, 2006 for a review), however, the mechanism of eruptive events is much less clear. The breakout has a key role in some events (Aulanier *et al.*, 2000; Gary and Moore, 2004; Sterling and Moore, 2004), the tether cutting in others (Sterling and Moore, 2003; Sterling and Moore, 2005) and the kink instability in yet another group (Török and Kliem, 2005). However, it is also possible that more than one one of these mechanisms may be involved in the same event (Williams *et al.*, 2005).

How are flares and CMEs related? The research on this question has a long history of controversy (see Harrison (1995) and Švestka (2001) for critical discussions of this subject). A consensus has emerged that CMEs and flares do not drive each other, but that they are rather different manifestations of a magnetic instability. However, the physical origin and spatial location of the flare(s) associated with a CME can be multiple. For example, reconnection can be present below (tether cutting) or above (breakout) the flux rope in the initial phase of the CME. In both cases reconnection is a possible trigger for the ejection. Reconnection is also expected below the erupting configuration as a consequence of the ejection. This is compatible with the continuous and broad distribution of flare properties (e.g. duration, intensity, relative location) found for flares associated with CMEs (Harrison, 1995). As individual detailed studies have shown (see previous paragraph), the flares associated with CMEs could have different origins, with the dominant mechanism changing from one event to the next. In this context we need further detailed studies of individual cases to improve our understanding.

We analyse here an event comprising a series of three flares occurring in close succession that have an associated CME and a clear quadrupolar configuration. The first two flares are impulsive and have characteristics of confined flares while the third is a long duration event (LDE). In the classical interpretation, this third flare would be associated with the launch of the CME. In fact, we demonstrate here that the two first flares are linked to the CME onset, while the third flare is only related to the relaxation of the coronal magnetic field after the CME has left the corona. We present a comprehensive study of this flare series and CME over a range of wavelengths and describe the evolving magnetic configurations that give rise to the event.

2. Flare and CME Observations

On the 20th January 2004 a three-phase event was observed with the GOES full-sun X-ray monitors. The light curve for this event is shown in Figure 1. The emission began to rise at around 07:32 UT and peaked at about 07:37 UT. The second phase began at approximately 07:40 UT, peaking at around 07:43 UT and decaying until 08:00 UT. At this time, the third and final phase of the sequence was observed as a Long Duration Event (LDE). This was a much smaller, C-class, flare rather than the two M-class flares that preceded it. It peaked just three minutes later and continued to decay until 11:00 UT. This sequence of flares was observed by imaging instruments in several different wavebands which allows us to investigate how the CME, which was observed by LASCO (Section 2.3), could have originated in association with two apparently confined flares (phases I and

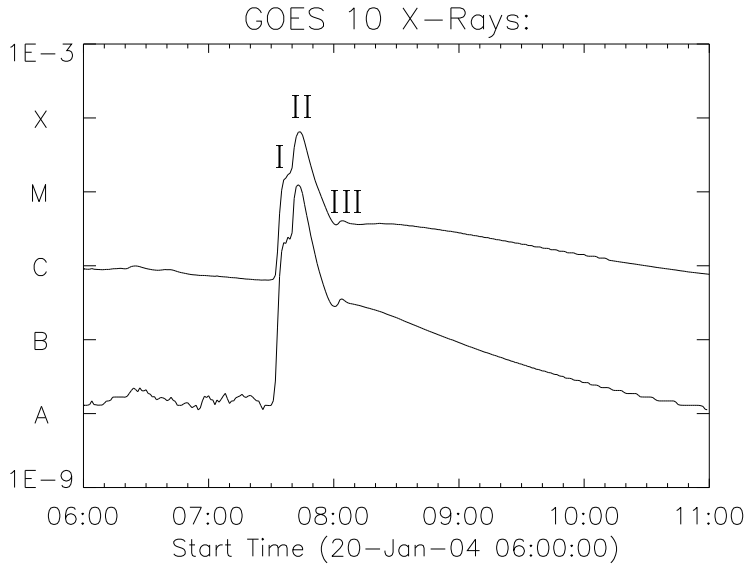

Figure 1. GOES light curve for the event on 20th January, 2004, at 07:32 UT. The three event phases are labeled (close to their maximum).

II). A classical interpretation would suggest an association with the LDE (phase III).

2.1. UV and Hα images of the flare sequence

The *Transition Region and Coronal Explorer* (TRACE) spacecraft (Handy *et al.*, 1999) was observing in the 1600 Å pass band during the event. The field of view covered the entire active region (AR) responsible for the flaring emission. It had a pixel size of $0.5''$ and a varying cadence between 3 and 60 s. Each frame was normalised for exposure time for direct comparison. There were two data gaps during the event when TRACE lost pointing. The first was between 07:33 UT and 07:51 UT during the transition between phases I and II, while the second followed phase III at 08:04 and ended at 08:37 UT. However, the Hα images from the Kwasan Observatory filled the first of these gaps (Figure 2). These images were digitized from film and formatted as a movie. Selected frames were aligned with the TRACE images using two sunspots as reference points. When the flare ribbons in these images were examined, the three phases of flaring could be clearly distinguished.

Figure 2 and movie (`traceHalpha.mpg`) illustrate the ribbon progression. The top left image from TRACE shows phase I. This was predominantly composed of two large ribbons to the east of the image with a smaller ribbon to the west ($x \approx 220''$, $y \approx -175''$). The image to the top right shows the same region in Hα and indicates the progression from east to

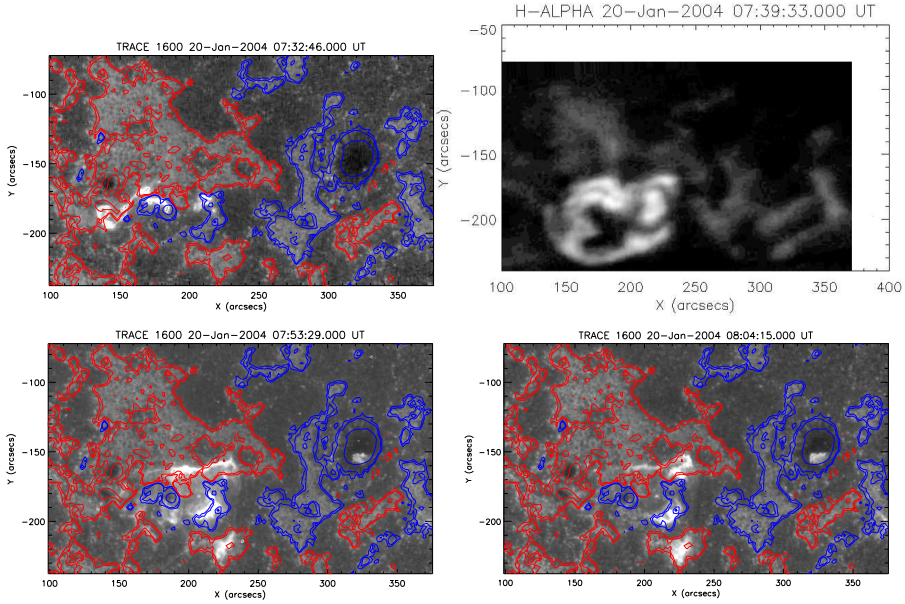

Figure 2. Images showing the three phase development of the event on 20th January, 2004, over the interval 07:32 UT to 08:04 UT. The *top left* (phase I) and the *bottom frames* (phases II and III) are TRACE 1600 Å observations with MDI magnetic field contours (± 50, 100, 500 G) overlaid, red/blue correspond to positive/negative values. The *top right frame* is a ground-based Hα image from Kwasan Observatory during the overlap of phases I and II. For clarification of ribbon development see the movie (`traceHalpha.mpg`) in the electronic version.

the west. This progression can be seen in both the north and the south. In the bottom left image, phase II is well under way following the data gap and the flare ribbons of phase I have faded. There were three ribbons in the centre and additionally there was a remote brightening in the western sunspot ($x \approx 325''$, $y \approx -145''$). Finally, in phase III, the two central ribbons extend to the west and in between the flare ribbons of phase II.

Using the TRACE images it is possible to study the temporal evolution of the emitted flux in different areas. In spite of the gap in TRACE data coverage, it is clear that during phase I there is a small amount of emission from regions that we later identify with phase II. Thus, phase II begins before phase I has ended with magnetic rearrangements overlapping in time as the energy release moves towards the west. This behavior is also evidenced in the light curves of Figure 1 from which it is clear that phases I and II overlap. A similar overlap is present between phase II and III.

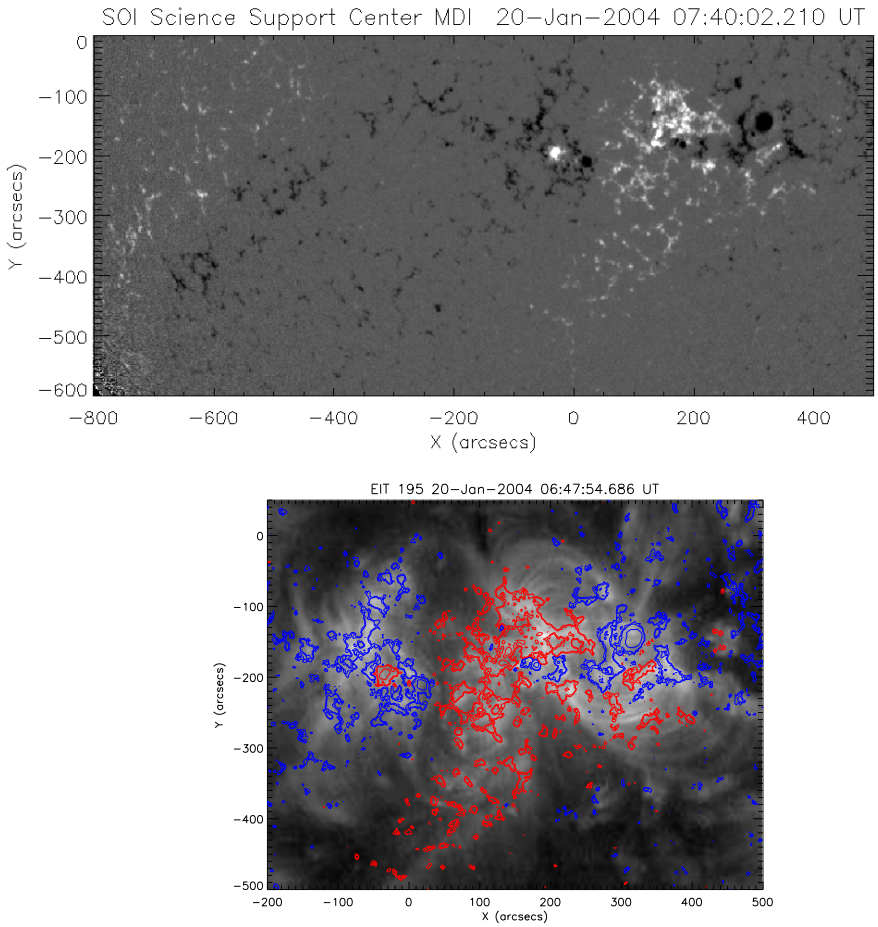

Figure 3. The *upper image* is a magnetogram from MDI showing, on the right, the flaring region (AR 10540) and a dispersed AR to the East that is associated with a large streamer. The *lower image* is taken by EIT at 6:47 UT, on which MDI isocontours (± 50, 100, 500 G) are overplotted. The field of view is a zoom on the right part of the top image to better show the coronal loops. The coronal loop connectivities are best visible within the AR.

2.2. Magnetic field observations

We analyse the magnetic evolution with magnetograms obtained by the *Michelson Doppler Imager* (MDI) on board the *Solar and Heliospheric Observatory* (SOHO, Scherrer *et al.*, 1995). An overview of the flaring region and the magnetic field concentrations to the east is given in one MDI magnetogram shown in Figure 3 (top frame). Below we show an overlay of an EIT image before the time of phase I and a part of the field of view of the previous MDI magnetogram. Large-scale connectivities can be seen within the flaring AR.

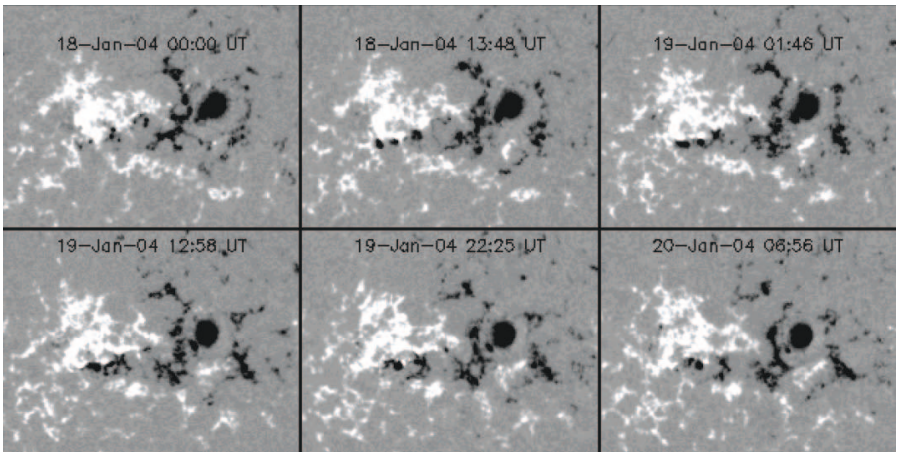

Figure 4. Sequence of MDI magnetograms showing the AR evolution from 18th to 20th January, 2004. The formation of several new bipoles is present along the south border of the dispersed positive polarity. For more details see the magnetic movie (`mdi.mpg`) in the electronic version.

During the period 18-20 January, 2004, numerous bipoles emerged leading to increased magnetic complexity within the active region (Figure 4 and `mdi.mpg`). In order to understand better the magnetic rearrangements involved, we have co-aligned the TRACE 1600 Å images with MDI magnetograms. As shown in Figure 2, the phase I ribbons were situated on either side of a magnetic neutral line, as expected. However, in phase II, the northernmost and southernmost ribbons lie in positive polarity fields, while the central ribbon is in a negative field region with an additional ribbon over the big leader spot which has negative polarity.

2.3. The related coronal mass ejection

The *Large Angle and Spectrometric Coronagraph* instrument (LASCO, Brueckner *et al.*, 1995) observed a CME in the C2 coronagraph. The CME leading edge was first visible in difference images at 08:06 UT, just minutes after the beginning of the LDE (phase III). In the plane of the sky the CME moved mainly southward with a slight eastward direction (Figure 5). This CME was clearly observed in running difference images, in both C2 and C3, and showed what appeared to be a traditional three-part structure. The leading edge was very faint and is difficult to see in a static image, but the core is clearly seen in Figure 5 (right) and in the LASCO/C2 movie (see the Appendix).

Height-time profiles were plotted from both the C2 and C3 data for the CME leading edge as well as for the core front edge (Figure 6). Measurements were made using a simple point and click method where the altitude is

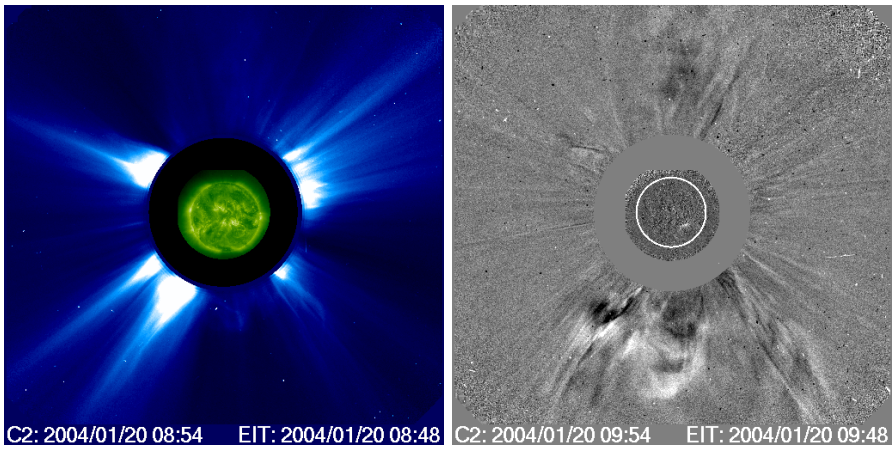

Figure 5. The images are from LASCO C2. *Left frame* shows the bright streamer, on the south-east. A faint southward CME was observed, starting at 08:06 UT on 20th January, 2004. The CME is better seen in the *right panel* in a running difference image. Note that the south-east streamer is disturbed by the CME (see the Appendix for movies).

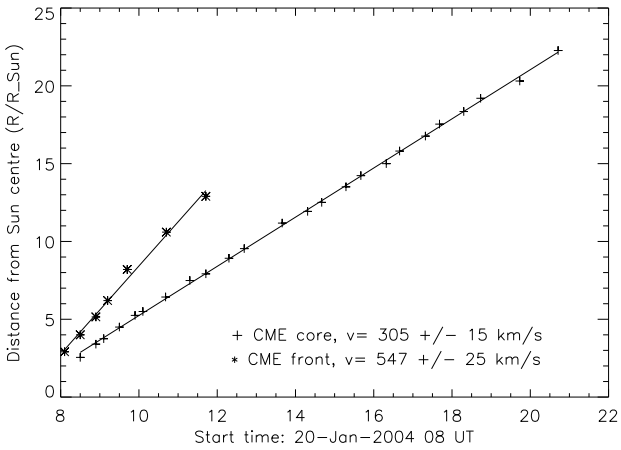

Figure 6. Distance-time plots for the CME core (crosses) and leading edge (asterisks) in LASCO/C2 and C3. The distance refers to the projection on the plane of sky of the radial distance from Sun centre. The error is the standard deviation in the fitting.

recorded along with the observation time. When measurements were repeated, the results were always within ± 5 pixels (57″ and 280″ for C2 and C3, respectively). No significant acceleration is apparent in either the C2 or the C3 images. The leading edge velocity, projected in the plane of sky, was between 502 km s^{-1} (in C3) and 560 km s^{-1} (in C2), while the core velocity was between 300 km s^{-1} (in C3) and 350 km s^{-1} (in C2). The combined height-time plot gave velocities of 547 ± 25 and 305

$\pm$ 15 km s^{-1}, respectively. If the CME were moving radially from its source origin ($\approx$W13 S12) for true velocity all those values should be multiplied by a factor of ≈ 3. In fact, the CME is seen moving slightly towards the east direction (Figure 5). This deviation from the radial direction is probably due to the stronger magnetic field within the AR compared with the weaker field towards the east (Figure 3). We have no further information on the CME trajectory, so the true CME speed cannot be determined.

On the eastern side of the CME, a streamer was rooted in the large dispersed negative field region (Figure 3). This streamer is observed to shift back and forth in the east-west direction as the CME propagates thus implying that there is an interaction between the two. This is clearly apparent when the data are viewed as a movie (see the Appendix).

2.4. Dimming and large scale loops

The SOHO *Extreme-ultraviolet Imaging Telescope* (EIT, Delaboudiniére *et al.*, 1995) was observing the solar disc with $\approx$ 12 minute cadence in the 195 Å (Fe XII) passband. These data allow us to determine the region from which the CME originated. By taking base difference images one can look for reduction in emission (long-term changes). This is referred to as an EIT dimming. The region is believed to dim as material leaves the field of view along open or expanded field lines, resulting in a decrease in density of emitting material (Hudson, Acton, and Freeland, 1996).

Dimmings were present around the flaring region. At approximately 08:00 UT, there was a significant dip in the light curve formed by summing the total emission of the AR. This dip lasted for nearly two hours. With running difference images it was also possible to see some of the magnetic loop structures with EIT. Following the flare activity, most of the flaring loops have an east-west orientation (Figure 7).

To the south-west of the AR there are large expanding loops which are moving away from the flare region (Figure 7, right arrow). This provides evidence for the expansion of the AR magnetic configuration. Magnetic reconnection is expected between this expanding structure and the neighbouring magnetic fields, in particular with the extended negative region (at the east of the AR, Figure 3). This reconnection implies the formation of interconnecting loops as observed with EIT (Figure 7, left arrow). The dark region shows that there was material present in the previous frame, while the bright region indicates that there is new material. This suggests that there are new interconnecting loops being formed and relaxing downwards. We also suggest that the streamer deflection (Section 2.3) is another consequence of this interaction.

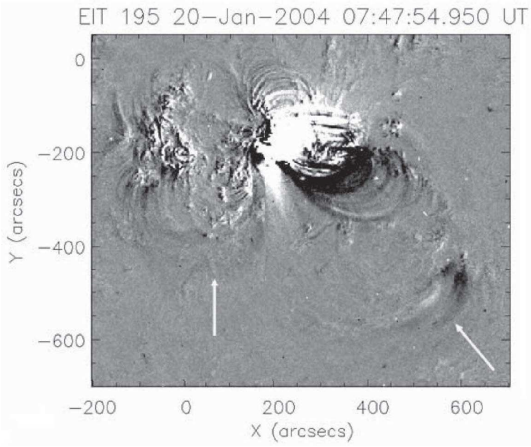

Figure 7. Running difference image showing the connection *(left arrow)* between the flaring region and the large dispersed negative polarity to the east. The difference is between the 07:47 UT and 07:35 UT images. This spans an interval from just after the start of phase I to just past the peak of phase II. *Right arrow* indicates a region with large expanding loops.

3. Flare-CME Connection

3.1. A classical CME-LDE relationship?

The time evolution seen in the GOES light curve is characteristic of two impulsive flares (phases I and II) followed by a third phase showing LDE characteristics (Figure 1). The TRACE images in conjunction with the MDI magnetograms indicated successive quadrupolar flare events for the three phases (Figure 2). The first phase has ribbons localized close to an S-shaped photospheric inversion line, just as seen in several previously analysed confined flares (see Démoulin (2006) for a review). In this case the flare would be due to magnetic reconnection between the emerging magnetic field and the pre-existing coronal field. This reconnection forms two lateral arcades without any eruption as described in the model of Melrose (1997). Thus, in a simple analysis, we concluded that the first two phases are confined flares and that phase III is associated with the CME.

However, a deeper investigation of the data shows inconsistencies in this interpretation. In particular, the LASCO observations show that the CME was launched before phase III (Figure 6). The linear (constant velocity) backward extrapolation of the CME projected distance-time profile, at the bottom of the corona and at the position of the AR on the disk ($\approx 0.3R_\odot$ from the disk centre), gives a starting time between 7:10 and 7:25 UT both for the core and leading edge of the CME. Taking into account a starting height of $\approx 0.3R_\odot$, delays the starting time by less than 2 min. But we have

also to take into account the fact that the CME was necessarily accelerating at these early times. This effect shifts the CME launch time to even earlier times than estimated above, so significantly before the beginning of phase I (around 7:32 UT).

There are two other pieces of evidence indicating that the eruption started earlier than phase III, as provided by radio observations analysed by Démoulin *et al.* (2007, Paper II). Firstly, two type II bursts were observed in the Culgoora dynamic spectrum (see Figure 1 in Paper II) starting as early as 7:39 UT, so just before the beginning of phase II. Type II bursts are considered to be radio signature of shock waves propagating through the corona. Secondly, they were preceded by a group of type III bursts (7:34-7:39 UT), which are usually observed at the beginning of an eruption. These bursts locate the start of the eruption at least at, and probably before, the beginning of phase I.

Unfortunately, in TRACE data the first data gap covers most of phase I and the beginning of phase II (between 7:33 and 7:51 UT). However, the first TRACE image after the gap shows that the western ribbons are well separated from the magnetic inversion line, in contrast to the last image before the gap (where ribbons are clustered around the inversion line). This large separation of the ribbons, characteristic of an eruption, is confirmed by Hα data even though the images are fuzzy (for more details, see movie `traceHalpha.mpg`).

Based on all this evidence, we conclude that the CME launch started before or at the beginning of phase I. It is likely that a slow expansion of the magnetic configuration began early and was significantly accelerated by the onset of a global magnetic instability.

3.2. Physical scenario for a multi-faceted event

Flare ribbons are thought to be indicators of the magnetic topology in any flaring configuration; the ribbons trace the chromospheric footpoints of the reconnected loops, and are located on one side of the separatrices or quasi-separatrix layers (QSLs). In the event studied here, the ribbons of the first two phases observed by TRACE, as well as those observed in Hα (Figure 2), have a spatial organization that is global in nature. They show basically two parallel ribbons on each side of the magnetic inversion line, and both ribbons end in hook shapes (Figure 8). Hα flare ribbons with a curved J-shape have been previously reported in several prominence eruptions and flares (e.g. Martin, 1979; Moore, Larosa, and Orwig, 1995; Pevtsov, Canfield, and Zirin, 1996; Williams *et al.*, 2005). This spatial organization of the ribbons is precisely the one found for the chromospheric trace of the QSLs in magnetic configurations which have a twisted core (Démoulin, Priest, and Lonie, 1996). It is important to note that both hook shapes are localized and curved

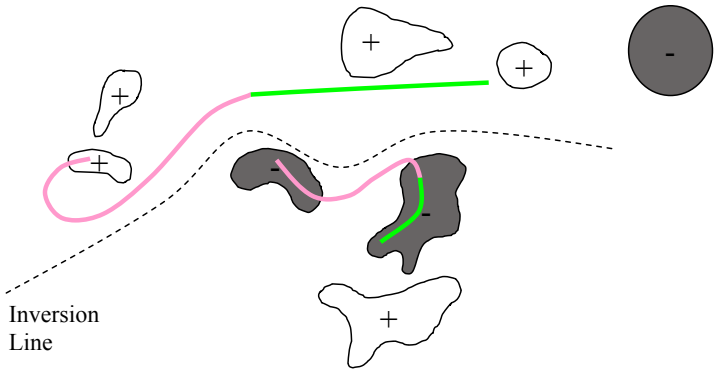

Figure 8. Schematic view of the main polarities and flare ribbons in phase I (pink) and II (green). This cartoon shows the global organization with two parallel ribbons shifted along the inversion line. Both ribbons are J-shaped, characteristic of a configuration with a twisted flux tube. Both the shift of the ribbons and the special location of the J-shape indicate a positive magnetic helicity.

so that they indicate a twisted flux tube with positive helicity, in agreement with the shift of the ribbons along the inversion line and the shear angle of coronal loops. It is unlikely that these hook shapes are the consequence of a special local magnetic field organization, both in the studied case and in previously reported ones.

Many eruptive events are associated with a classical two ribbon flare in which the ribbons are separating with time (e.g. Moore *et al.*, 2001; Asai *et al.*, 2003; and references therein), while some others show a progression of flare brightening along the inversion line together with a separation of the ribbons (e.g. in the Bastille day flare, Fletcher and Hudson, 2001). Yet others show mainly a shift along the inversion line (e.g. Grigis and Benz, 2005). The case studied here is of the second type with the particular feature that the main site of magnetic reconnection progresses stepwise along the inversion line. This is probably due to the multi-flux tube emergence observed before flaring (Figure 4), which strongly modulates the magnetic configuration along the inversion line.

With the above considerations, as synthesized in Figure 9, phases I and II are related to a series of steps involving tether cutting. Magnetic reconnection progressively transforms the sheared arcade to a twisted flux tube, which becomes unstable and erupts.

At first sight, phase I could be viewed as an energetic version of the flare precursor of the CME as found by Harrison *et al.* (1985) and Harrison (1986). However, phase I is not a typical precursor since it overlaps with phase II. In addition, phase I does not occur prior to the launch of the CME since the backward extrapolation of the height-time plot suggests an earlier

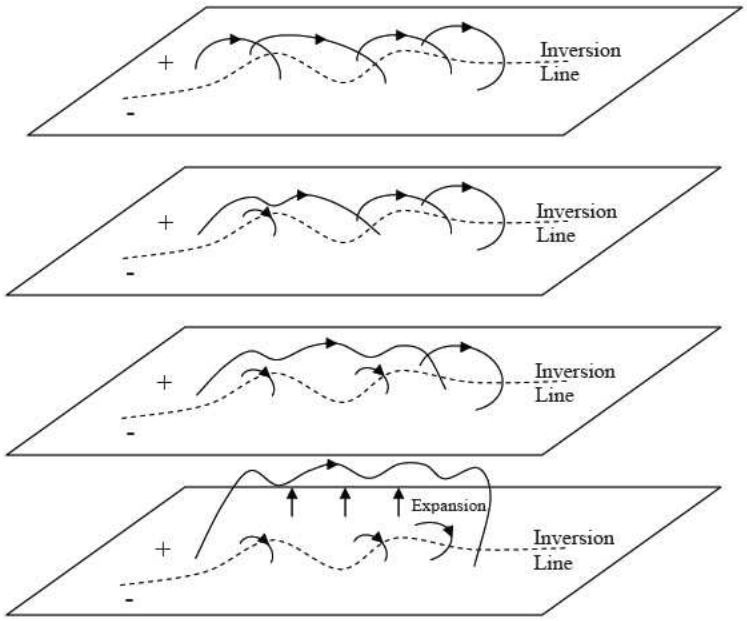

Figure 9. Cartoons summarizing the change in magnetic connectivities as deduced from the flare observations. The evolution of the ribbons is due to the 'propagation' of reconnection from east to west. Reconnection in the magnetic arcade progressively builds a twisted flux tube, which becomes unstable leading to the CME. *Top panel:* initial sheared configuration; *middle panels*: connectivities during phase I and at the beginning of phase II; *bottom panel:* the flux rope fully erupts.

departure time for the CME (Section 3.1). So, even if the first brightenings are observed in phase I, it cannot be considered as a precursor since it belongs to the process of the CME launch.

3.3. Reconnection with neighbouring fields

As the magnetic configuration erupts, it finds weaker magnetic fields in the surrounding corona, then it rapidly expands. Current sheets are expected to form between fields of different orientations pushed against each other. Then, when the currents are intense enough, magnetic reconnection starts. This occurred predominantly towards the eastern and western regions, as described below.

The erupting field reconnects with the eastern open field present over the extended negative polarity (evidenced by the presence of a streamer in Figure 5). This reconnection implies the formation of new loop connections between AR 10540 and the negative polarity to the east, as observed with EIT (Figure 7). Evidence for such a connection is also found in magnetic extrapolation of an MDI magnetogram (Figure 10). The other set of re-

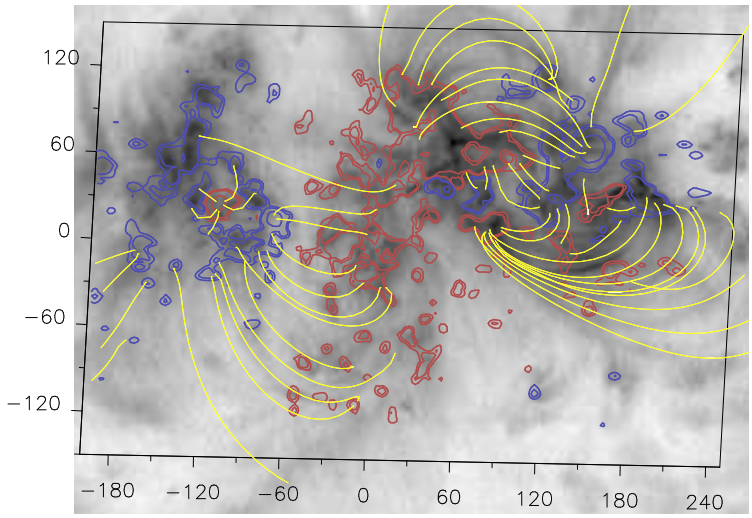

Figure 10. Magnetic extrapolation computed with a linear force-free field. The yellow lines show the connectivities within AR 10540 and between the two active regions overlaid on an EIT image at 06:47 UT. The large scale field has a negative α-value (so helicity), which is the opposite from the newly emerging bipole associated to the flares (Figure 8). Blue and pink lines are isocontours of the vertical magnetic field component ($\pm 50, 100, 500$ G).

connected field lines is connected to the interplanetary space. This allows accelerated electrons to escape and to create the observed type III bursts (Section 3.1). This reconnection occurred at the beginning of phase I, so close to the CME launch time. It also removed the confinement of surrounding loops. It thus shows the expected characteristics for the first reconnection step occurring in the breakout model. However, the backward extrapolation of the CME trajectory (Section 3.1) is an indication that the CME started earlier.

The erupting field also reconnects with the neighbouring field present towards the south-west. The observed flare ribbons on the west side (indicated by arrows on Figure 11) provide observational evidences of this magnetic energy release in the corona. Energy was partly transported towards the chromosphere along reconnected magnetic field lines. Faint connecting loops, mostly unresolved, can be seen in the TRACE movie both in phases II and III between the two main ribbons (in particular, compare phase III with the period after the data gap, when the flare ended).

This forced reconnection process in phase II is sketched in the top panel of Figure 12. Both blue lines represent the typical pre-reconnection magnetic field lines. Since it is the external part of the erupting field which is reconnected, the reconnecting field lines are expected to be nearly potential arcade-like. The forced reconnection produces two new sets of connections (in red) and leads to the creation of four extra ribbons (Figure 11). These

Figure 11. TRACE 1600 Å images taken at 8:00 and 8:03 UT in phases II and III, respectively. The four flare ribbons, which are sketched in Figure 12, are indicated by arrows.

ribbons are represented by short black lines in Figure 12. Only two of them are clearly separated from the two main ribbons of the eruption: the western and the southern ones close to the leading spot and in the southern positive facular region (see Figure 11). Evidence of the other two can be found by a careful study of the TRACE movie as a western extension of the main ribbons.

Later on, in phase III, the western end of the two main ribbons extends in a complex and non-standard way (see `traceHalpha.mpg` in the electronic supplement). After exploring different scenarios, we conclude that the one in best agreement with the observations is a relaxation scenario with the following steps. The expansion of the erupting field has transferred flux to the lateral connections (red lines in the top panel of Figure 12), but when the erupting field is far away, there is no longer a large magnetic pressure to sustain such forced connectivities. Indeed, the field in the erupting region re-

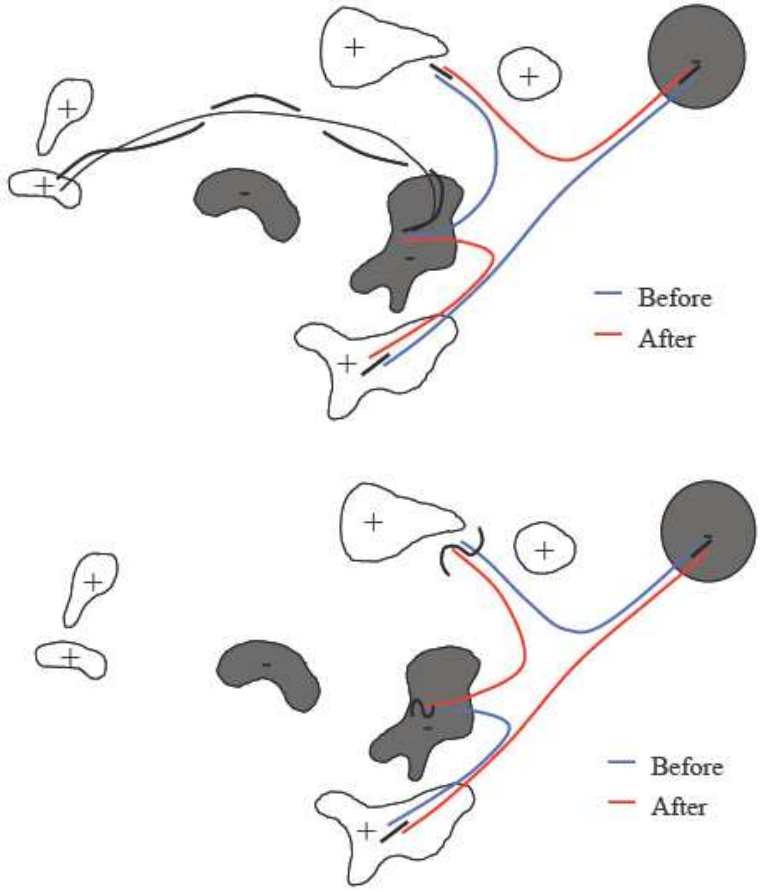

Figure 12. Interpretation of the western ribbons seen in phases II and III (cf. Figure 11) due to the reconnection of the erupting configuration with the magnetic field towards the west. The main polarities are represented as in Figure 8. *Black lines* on the left represent the erupting twisted configuration. The four short *thick black lines* represent the observed ribbons (cf. Figure 11 and `traceHalpha.mpg`). *Blue lines* show pre-reconnection, *red lines* post-reconnection magnetic connectivities, as needed to interpret the ribbon locations. Only the ribbons and the magnetic polarities are observed; therefore, the magnetic field connections are deduced from the flare ribbon locations (Section 3.3) with the help of magnetic extrapolations (Figure 10). The *top panel* shows the reconnection process during phase II forced by the erupting (expanding) flux rope when it encountered large-scale magnetic loops connecting the large leading spot and a southern facular area. The *lower panel* shows the change of connectivities during phase III, when magnetic reconnection proceeds in the reverse way from the previous step (this relaxation occurs since too much flux was forced to reconnect by the erupting flux tube).

laxes and forms low-lying loops with less magnetic shear. The large magnetic pressure built in the lateral connections can now drive magnetic reconnection in the opposite direction (bottom panel of Figure 12). This reverse reconnection process probably creates the puzzling ribbon extensions on the western side of the two main ribbons in phase III. An analogous phenomenon, though in a very different magnetic configuration, was observed in a large flare event (Gary and Moore, 2004; Harra *et al.*, 2005). Such relaxation reconnection, after forcing, is likely to be a general phenomenon, which so far has been largely overlooked.

We conclude that phase III is associated with relaxation to a more potential configuration after the CME departure giving a classical two-ribbon flare as it was found in many LDEs (e.g. Tsuneta *et al.*, 1992; Harra-Murnion *et al.*, 1998; Švestka, 2001). However, phase III is also related to the amount of reconnection with the surrounding fields. In the present event, the latter reconnection occurs with strong magnetic field within the same AR. It is expected that phase III would have been less intense if the full AR magnetic field had been involved in the CME, since the strong surrounding fields would have been located in another, more distant, AR, the reconnection would have been less efficient. This could explain that there is not a simple relationship between CMEs and LDEs (Harrison, 1995): we suggest that, for our event at least, the strength of the LDE depends on the magnetic environment of the erupting configuration (keeping in mind that there is also another reconnection associated to the classical two-ribbons and the relaxation of the erupting configuration by itself).

4. Conclusions

The event of the 20th January 2004 was challenging to understand since it had several unusual components. The flare had three phases, separated both temporally and spatially, but also with an overlap and physical connection between consecutive phases. Each phase had four main flare ribbons with configurations similar to previously analysed confined flares. However, a CME was observed originating from this AR at the time of these flares, and its relationship with the flare phases was puzzling. Furthermore, a group of type III, two type II bursts and a decametric-hectometric N burst were also associated with this event (see Paper II). Due to the complexity of the event, it was difficult to clearly distinguish the processes at the heart of the eruption from the side effects.

After exploring several physical scenarios, we have included all the observed constraints in a coherent physical framework. The successive observed flare events were a consequence of the emergence of several magnetic bipoles in the pre-existing bipolar AR 10540. The re-organization of the magnetic

field by tether cutting provides one plausible origin for the instability of the magnetic configuration leading to the CME. Magnetic reconnection proceeds stepwise, along the inversion line formed by the new bipoles, producing the first two flares.

The erupting (expanding) magnetic configuration interacted and reconnected with neighbouring open fields, creating new interconnecting loops, type III bursts and an N burst. These radio bursts are present at the beginning of the first flare phase. They are associated with the removal of arcade-like field lines above the erupting configuration by reconnection with open field lines. This process then decreases the stability of the magnetic configuration. It is a version of the breakout model, with a current layer formed between the core field and surrounding open field lines.

The extrapolation backward in time of the CME trajectory points to an initiation of the CME at even earlier times than the observed type III bursts and phase I (by at least 10 minutes). This suggests the following sequence of events. First, the magnetic configuration expanded. This is followed by its reconnection with nearby open field lines (giving the type III burst) and phase I with tether cutting reconnection. Then, magnetic reconnection drifts along the magnetic inversion line in phase II. We interpret both phases as the progressive transformation of the arcade-like configuration to a twisted flux tube (Figure 9). Note that a twisted flux tube could have been present before these phases, but we have no observational evidence of it. If this is the case, the flux rope is simply growing in flux and twist in these phases. Finally, this magnetic configuration left the corona, giving rise to the CME.

We find evidence that the third flare, an LDE, is due to the relaxation of the magnetic configuration after the CME is launched towards the interplanetary space. More precisely, in addition to the classical two-ribbon flare process, the expanding magnetic structure of the CME forces magnetic reconnection with the surrounding fields within the AR. When the CME has left the corona, i.e. when the forcing disappears, a long-duration reverse reconnection begins.

This event illustrates the complexity of the relationship between flares and CMEs. Depending on the amount of reconnected magnetic field in the different phases, the CME can be associated with an impulsive or with an LDE flare, with all the variants a priori possible between these two extremes (even with multi-peaks in the X-ray emission). One of the associated flares can be a precursor around the main inversion line (tether cutting reconnection) or located at larger scales (breakout). An LDE flare, whose classical behaviour is related to two-ribbon flaring, can also be expected as a consequence of the relaxation of the magnetic configuration. However, its intensity can also be greatly affected by the amount of reconnection with neighbouring magnetic fields not involved in the instability that caused the CME. These characteristics permit considerable flexibility in the location,

duration and intensity of the associated flares. All these points are consistent with the statistical study of Harrison (1995) showing the large variety of physical properties of flares associated with CMEs.

This complex event illustrates, even better than any of our previous studies, the necessity for multi-instrument and multi-wavelength data to understand the physics involved. For example, with only coronal data, we would have concluded that the two first impulsive flares were due to local magnetic reconnection with only low coronal implications. The multi-wavelength data also permits us to understand that the CME was in fact related to the first phases, although both are impulsive M flares, and that the third phase, with LDE characteristics, was merely the relaxation phase of the magnetic configuration.

Acknowledgements

The authors are grateful to the referee for helpful comments. The authors thank the SOHO/MDI, LASCO, EIT and TRACE consortia for their data. The CME movies are from the CME catalog generated and maintained at the CDAW Data Center by NASA and The Catholic University of America in cooperation with the Naval Research Laboratory. SOHO is a joint project by ESA and NASA. C.H.M. is grateful for an PPARC funded visitor's grant. C.H.M. acknowledges support from the Argentinean grants: UBACyT X329 (UBA), PICT 12187 (ANPCyT) and PIP 6220 (CONICET). C.H.M. and P.D. acknowledge financial support from CNRS (France) and CONICET (Argentina) through their cooperative science program (05ARG0011, N^0 18302). L.V.D.G. acknowledges the Hungarian government grant OTKA 048961. J.L.C. thanks the Leverhulme Trust for the award of a Leverhulme Emeritus Fellowship. We thank Jian Sun for his help in improving the TRACE-Hα movie.

Appendix

Movies of the magnetic field evolution (`mdi.mpg`) and flare ribbons evolution (`traceHalpha.mpg`) are available in the electronic version of this paper. In the TRACE-Hα movie, the intensity of the TRACE images was not fully calibrated (there is a roll over at high values). However, the intensity was fully calibrated for Figure 2. The running difference movies of the CMEs observed by LASCO C2 and C3 (`c2_rdif.html`, `c3_rdif.html`) are available from
`http://cdaw.gsfc.nasa.gov/CME_list/daily_movies/2004/01/20/`

References

Amari, T., Luciani, J.F., Aly, J.J., Mikic, Z., and Linker, J.: 2003, *Astrophys. J.* **585**, 1073.

Antiochos, S.K., DeVore, C.R., and Klimchuk, J.A.: 1999, *Astrophys. J.* **510**, 485.

Asai, A., Ishii, T.T., Kurokawa, H., Yokoyama, T., and Shimojo, M.: 2003, *Astrophys. J.* **586**, 624.

Aulanier, G., DeLuca, E.E., Antiochos, S.K., McMullen, R.A., and Golub, L.: 2000, *Astrophys. J.* **540**, 1126.

Brueckner, G.E. *et al.*: 1995, *Solar Phys.* **162**, 357.

Delaboudiniére, J.P. *et al.*: 1995, *Solar Phys.* **162**, 291.

Démoulin P.: 2006, *Adv. Space Res.* **37**(7), 1269.

Démoulin, P. *et al.*: 2007, *Solar Phys.*, in press (Paper II).

Démoulin, P., Priest, E.R., and Lonie, D.P.: 1996b, *J. Geophys. Res.*, **101**, 7631.

Démoulin, P., van Driel-Gesztelyi, L., Schmieder, B., Hénoux, J. C., Csepura, G., and Hagyard, M.J.: 1993, *Astron. Astrophys.* **271**, 292.

Fletcher, L. and Hudson, H.: 2001, *Solar Phys.* **204**, 69.

Gary, G.A. and Moore, R.L.: 2004, *Astrophys. J.* **611**, 545.

Grigis, P.C. and Benz, A.O.: 2005, *Astrophys. J.* **625**, L143.

Handy, B.N. *et al.*: 1999, *Solar Phys.* **187**, 229.

Harra-Murnion, L.K.*et al.*: 1998, *Astron. Astroph.* **337**, 911.

Harra, L.K. *et al.*: 2005, *Astron. Astrophys.* **438**, 1099.

Harrison, R.A.: 1986, *Astron. Astrophys.* **162**, 283.

Harrison, R.A.: 1995, *Astron. Astrophys.* **304**, 585.

Harrison, R.A. *et al.*: 1985, *Solar Phys.* **97**, 387.

Hudson, H.S., Acton, L.W., and Freeland, S.L.: 1996, *Astrophys. J.* **470**, 629.

Inhester, B., Birn, J., and Hesse, M.: 1992, *Solar Phys.* **138**, 257.

Lin, J., Forbes, T.G., Isenberg, P.A., and Démoulin, P.: 1998, *Astrophys. J.* **504**, 1006.

Mandrini, C.H., Démoulin, P., Hénoux, J. C., and Machado, M. E.: 1991, *Astron. Astrophys.* **250**, 541.

Martens, P.C.H. and Kuin, N.P.M.: 1989, *Solar Phys.* **122**, 263.

Martin, S.F.: 1979, *Solar Phys.* **64**, 165.

Melrose, D.M.: 1997, *Astrophys. J.* **486**, 521.

Moore, R.L., Larosa, T.N., and Orwig, L.E.: 1995, *Astrophys. J.* **438**, 985.

Moore, R.L., Sterling, A.C., Hudson, H.S., and Lemen, J.R.: 2001, *Astrophys. J.* **552**, 833.

Nitta, N.V. and Hudson, H.S.: 2001, *Geophys. Res. Lett.*, **28**(19), 3801.

Pevtsov, A.A., Canfield, R.C. and Zirin, H.: 1996, *Astrophys. J.* **473**, 533.

Scherrer, P.H. *et al.*: 1995, *Solar Phys.* **162**, 129.

Sheeley, N.R., Jr., Howard, R.A., Koomen, M.J., and Michels, D.J.: 1983, *Astrophys. J.* **272**, 349.

Shiota, D., Isobe, H., Chen, P.F., Yamamoto, T.T., Sakajiri, T., and Shibata, K.: 2005, *Astrophys. J.* **634**, 663.

Sterling, A.C. and Moore, R.L.: 2003, *Astrophys. J.* **599**, 1418.

Sterling, A.C. and Moore, R.L.: 2004, *Astrophys. J.* **602**, 1024.

Sterling, A.C. and Moore, R.L.: 2005, *Astrophys. J.* **630**, 1148.

Švestka, Z.: 1989, *Solar Phys.* **121**, 399.

Švestka, Z.: 2001, *Space Sci. Rev.* **95**, 135.

Török, T. and Kliem, B.: 2003, *Astron. Astrophys.* **406**, 1043.

Török, T. and Kliem, B.: 2005, *Astrophys. J.* **630**, L97.

Tsuneta, S. *et al.*: 1992, *Publications of the Astronomical Society of Japan* **44**, L63.

van Ballegooijen, A.A. and Martens, P.C.H.: 1989, *Astrophys. J.* **343**, 971.

Webb, D.F. and Hundhausen, A.J.: 1987, *Solar Phys.* **108**, 383.
Williams, D.R., Török, T., Démoulin, P., van Driel-Gesztelyi, L., and Kliem, B.: 2005, *Astrophys. J.* **628**, L163.